MDPI

Article

Model-Based Design and Operational Optimization of HPC Waste Heat Recovery and High-Temperature Aquifer Thermal Energy Storages in Existing Energy Infrastructures

Niclas Hampel [1], André Xhonneux [1,*] and Dirk Müller [1,2]

[1] Forschungszentrum Jülich GmbH, Institute of Climate and Energy Systems, Energy Systems Engineering (ICE-1), 52425 Jülich, Germany ; n.hampel@fz-juelich.de (N.H.)
[2] E.ON Energy Research Center, Institute for Energy Efficient Buildings and Indoor Climate, RWTH Aachen University, 52056 Aachen, Germany; dmueller@eonerc.rwthaachen.de (D.M.)
* Correspondence: a.xhonneux@fz-juelich.de (A.X.)

Abstract

The waste heat generated by high-performance computing (HPC) represents an opportunity for advancing the decarbonization of energy systems. Seasonal storage is necessary to regulate the balance between waste heat production and demand. High-temperature aquifer thermal energy storage (HT-ATES) is a particularly well-suited technology for this purpose due to its large storage capacity. However, integrating HT-ATES into energy systems for district heating is complex, affecting existing components. Therefore, this study applies a bi-objective mixed-integer quadratically constrained programming (MIQCP) approach to optimize the energy system at Forschungszentrum Jülich (FZJ) regarding total annualized costs (TAC) and global warming impact (GWI). The exascale computer *Jupiter*, which is hosted at FZJ, generates a substantial amount of renewable waste heat that is suitable for integration into district heating networks and seasonal storage. Case studies show that HT-ATES integration into the investigated system can reduce GWI by 20 % and increase TAC by 1 % compared to the reference case. Despite increased TAC from investments and heat pump (HP) operation, summer charging of the HT-ATES remains flexible and cost-effective. An idealized future scenario indicates that HT-ATES with a storage capacity of 16 990 MWh and HPs could cover most of the heating demand, reducing GWI by up to 91 % while TAC increases by 6 % relative to the reference system.

Keywords: high-temperature aquifer thermal energy storage; district heating; mixed-integer quadratically constrained programming; waste heat utilization; high-performance computing; design and operational optimization

Received:
Revised:
Accepted:
Published:

Citation: Hampel, N.; Xhonneux, A.; Müller, D. Title. *Energy Storage Appl.* **2025**, *1*, 0. https://doi.org/

1. Introduction

Decarbonization presents novel challenges for energy systems, necessitating both a transition from fossil fuels to renewable energies and the coupling of multiple energy sectors. A considerable number of governments have prioritized the reduction of greenhouse gas (GHG) emissions, with this objective being formally established in the EU Climate Law [1]. The overarching aim of this legislative instrument is to achieve net zero emissions by the year 2050. At the same time, energy demand is rising sharply due to advancing digitalization and the increasing deployment of artificial intelligence (AI) technologies. In 2024, global data centers consumed an estimated 460 TWh of electricity and this share is expected to double by 2030 [2]. As a byproduct, a significant amount of waste heat is

produced, which represents substantial potential for the decarbonization of energy systems [3]. Especially high-performance computing (HPC) consume large amounts of electrical energy and continuously generate waste heat which can be used for district heating [4]. As is the case with renewable energies, a discrepancy between production and demand is evident on a seasonal basis. Long-term thermal energy storage systems offer a key technology for seasonal decoupling of production and demand. A variety of long-term storage options exist, including borehole, pit and aquifer thermal energy storage (ATES) systems. Compared to borehole or pit storage systems, ATES systems have the lowest capital costs per storage volume and energy [5]. Furthermore, it has been recently shown that ATES, storing waste heat from a data center among other sources, can reduce emissions by up to 74% with heat pumps (HPs) compared to systems based on heating oil or natural gas [6]. For the storage process, the circulation of water is facilitated by a pump in conjunction with one or more pairs of wells, thus enabling seasonal heating. Since the efficiency, losses and capacity of ATES is highly dependent on the local conditions of the subsurface such as permeability and groundwater velocity, the general suitability of the subsurface must be examined. A further distinction must be made between low-temperature (LT)-ATES, which range up to 25°C, and high-temperature (HT)-ATES, which range from 50°C [7]. While LT-ATES are mostly used for heating and cooling of several buildings in combination with HPs, HT-ATES can be used for district heating [7].

1.1. State of the Art

Almost 3500 ATES systems exist worldwide, 85% of which are located in the Netherlands [8,9]. In Germany there are only a few commercial plants in Rostock and Bonn due to a lack of incentive programs, insufficient knowledge and only less pilot plants [7]. Therefore, numerous research projects are still in the early stages of development, whereby the research interest has increased in recent years [10]. The majority of these projects are confined to the research of location potential and numerical simulations. Numerical modeling approaches are essential for implementing ATES, investigating thermal, hydraulic and chemical processes [11]. These approaches are further important for simulations about temperature profiles in the wells or storage losses. However, they do not take into account the economic or ecological performance of the ATES. Therefore, techno-economic analyses that consider competing technologies and local market conditions are crucial [10]. Daniilidis et al. [12] conducted a techno-economic assessment of an HT-ATES system in Switzerland and found that a minimum capacity of around 25 MW is required to achieve competitiveness with large-scale district heating networks. With a transmissivity of at least $2.5 \cdot 10^{-12} \mathrm{m}^3$, the levelized cost of heat can be kept below 200 CHF/MWh, potentially enabling a CO_2 reduction of 0.8 billion kg over 15 years. Schüppler et al. [13] analyzed an LT-ATES integrated into a hospital energy system in Karlsruhe, reporting a payback period of only three years despite 50% higher capital costs, alongside annual CO_2 savings of approximately 600 t. Todorov et al. [14,15] investigated the integration of an ATES with a groundwater heat pump in Finnish district heating and cooling networks, demonstrating economic feasibility with production costs between 30 and 41.5 €/MWh and limited environmental impacts over a 20-year operation period.

Nonetheless, the successful integration of an ATES into existing energy systems fundamentally requires consideration of the interactions between their individual components. Ensuring the efficient operation of the entire system, in terms of both costs and emissions, is essential. Consequently, optimization approaches are well-suited for identifying the optimal operation and design strategy for energy systems that incorporate ATES. Perera et al. [16] performed a multi-objective optimization regarding costs, grid integration level and fuel consumption for ATES integration into a distributed energy system. They showed that

ATES are suitable to improve the renewable grid integration level and minimize the dependence on fossil fuels. Verheyen et al. [17] used a mixed-integer linear programming (MILP) approach to model ATES behaviour in district energy systems. They investigated the ATES in different scenarios and concluded that ATES integration is not always favourable regarding costs or emissions. However, they have seen that the ATES leads to more renewable heat supply from solar thermal in all scenarios.

The previous studies have optimized energy systems incorporating ATES using industrial waste heat or solar thermal energy to improve flexibility and reduce emissions in energy systems. However, research on ATES systems utilizing waste heat from data centers or HPC is lacking, despite their increasing relevance to modern energy systems, as previously indicated. For instance, Dvořak et al. [18] conducted a simulation-based assessment of integrating data center waste heat into an existing ATES system on a university campus, demonstrating significant potential for energy savings and CO_2 reduction of 680 t per year on average for the current ATES policy. In a future scenario, the ATES can improve the CO_2 reduction by 1000 t per year on average. Leindals et al. [19] applied context-aware reinforcement learning to optimize the cooling operation of data centers coupled with an ATES system, demonstrating improvements in thermal stability and energy management. However, most studies on ATES with data center waste heat are limited to either local simulations or operational control. Consequently, there is a lack of optimization approaches for large-scale energy systems incorporating ATES charged by waste heat generated from data centers or HPC, respectively. As previously mentioned, optimization is important when integrating ATES into large energy systems for district heating due to the complex interaction with other system components.

1.2. Contribution

The novelty of this work consists in the bi-objective optimization of the design and operation of a large-scale energy system with an ATES charged by renewable waste heat of HPC. Since HT-ATES are the most appropriate storage technology for large-scale district heating networks [20], an HT-ATES will be studied in this work. At Forschungszentrum Jülich (FZJ) the geological conditions for an HT-ATES are given based on a preliminary study. Furthermore, the exascale computer *Jupiter* is already operational and could deliver waste heat up to 18 MW with a temperature of approximately 40 °C. Due to the high supply temperatures of the local district heating network (90-120 °C) the waste heat has to be conditioned by industrial HPs to reach usable temperature levels. Besides the direct waste heat utilization, the waste heat can be employed indirectly by conditioning it with the HPs in summer, storing it in the HT-ATES and retrieving it in winter. In the long-term, one option to replace the fossil heat sources of the FZJ could be the direct waste heat utilization in combination with HPs and HT-ATES. The present study investigates the HT-ATES integration by focusing on the following aspects:

- Development of a mixed-integer quadratically constrained programming (MIQCP) model for optimizing the design and operation of an energy system with HT-ATES
- Integration of renewable HPC waste heat as a thermal source for the HT-ATES within a district heating network
- Bi-objective optimization of annual costs and CO_2 emissions at the system level

The paper is structured as follows: Section 2 gives an overview of the existing FZJ energy system and the corresponding model and describe the model extensions for HPC, HP and HT-ATES. Furthermore, the objective functions total annualized costs (TAC) and global warming impact (GWI) are introduced. Section 3 describes the data preparation and clustering of the dataset for the case studies. Additionally, an overview of investigated case studies and sensitivity analyses is presented as well as the solution approach of the

optimization problem. Section 4 provides the optimization results as Pareto fronts for the case studies and sensitivity analyses. In Section 5, the results are discussed from economic and ecological perspectives. Finally, the main outcomes are summarized in Section 6.

2. Materials and Methods

In this chapter, the models for the current and the extended energy system are introduced. The extended energy system includes models of the HP, ATES and waste heat source (WH) as well as the linking component model. Furthermore, the objective functions TAC and GWI are described. The modeling and optimization of the energy system is done with the object-oriented open-source framework COMANDO [21] which is based on the two-stage stochastic programming approach. This approach allows the simultaneous design and operational optimization of energy systems.

2.1. Current Energy System

The current FZJ energy system (Figure 1) is characterized by the combined cooling, heating and power (CCHP) self production with natural gas from the gas grid (GG). The thermal-led CCHP consists of three combined heating and power (CHP) plants, two boilers and one absorption chiller. The thermal demand is mainly covered by the CHP plants, whereby the boilers cover peak loads. The absorption chiller absorbs surplus heat and therefore ensures the generation of surplus electricity of the CCHP, especially in summer.

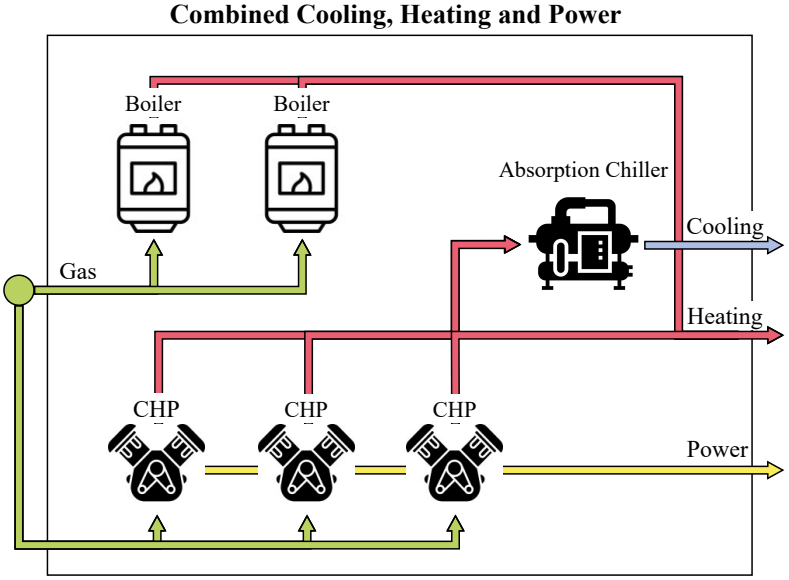

Figure 1. Structure of the CCHP of the FZJ consisting of three CHP units, two boilers and one absorption chiller. The entire CCHP system has been designed for thermal demand management.

The quasi-stationary models for the already existing components (Figure 2, left) are implemented based on previous work [22,23] and are therefore presented in abbreviated form. Fundamental are the following equality and inequality constraints for boiler, CHP, absorption chiller and compression chiller models:

$$\dot{Q}_{out} = \eta_{heat/cool}(\lambda) \cdot \dot{Q}_{in} \tag{1}$$

$$\dot{Q}_{out} = \lambda \cdot \dot{Q}_{nom} \tag{2}$$

$$\dot{Q}_{min} \leq \dot{Q}_{nom} \leq \dot{Q}_{max} \tag{3}$$

$$\lambda_{min} \leq \lambda \leq 1 \tag{4}$$

For the CHP, the electric output is also defined as:

$$P_{out} = \eta_{el}(\lambda) \cdot \dot{Q}_{in} \tag{5}$$

Where $\dot{Q}_{out}$ and P_{out} denotes the thermal and electrical output which depend on the thermal and electrical efficiencies $\eta_{heat/cool}$ and η_{el}, as well as the part load λ. Note that η is the coefficient of performance (COP) for chillers and HPs, which is not necessarily temperature independent [22,24]. Based on [23], following values are chosen for the components with several simplifications: One boiler has a nominal thermal power of 16 MW with an assumed constant thermal efficiency of 80 % and a minimal part load of 20 %. Both have the function to cover peak heating demands. The three CHPs have each a nominal electric power of 4.3 MW with efficiency values of $\eta_{heat} = 0.437$ and $\eta_{el} = 0.432$ at 100 % load. The part-load efficiency is linearly approximated. The minimal part load is set to 50 %. The installed absorption chiller has a nominal cooling power of 5.7 MW and provides cooling in addition to the compression chillers as central cooling supply with a power of 21 MW. However, the primary role of the absorption chiller is to ensure a stable running of the CHP during summer and to increase full-loads hours, thereby enabling a substantial share of the electricity to be self generated at affordable prices. The COP part load curve is modelled according to manufacture specifications and the minimal part load is set to 20 %. Due to the lack of detailed data and the presence of a mix of different compression chillers, the COP of the compression chiller is assumed to be constant at 3.7 and part-load behaviour and maintenance costs are negligible.

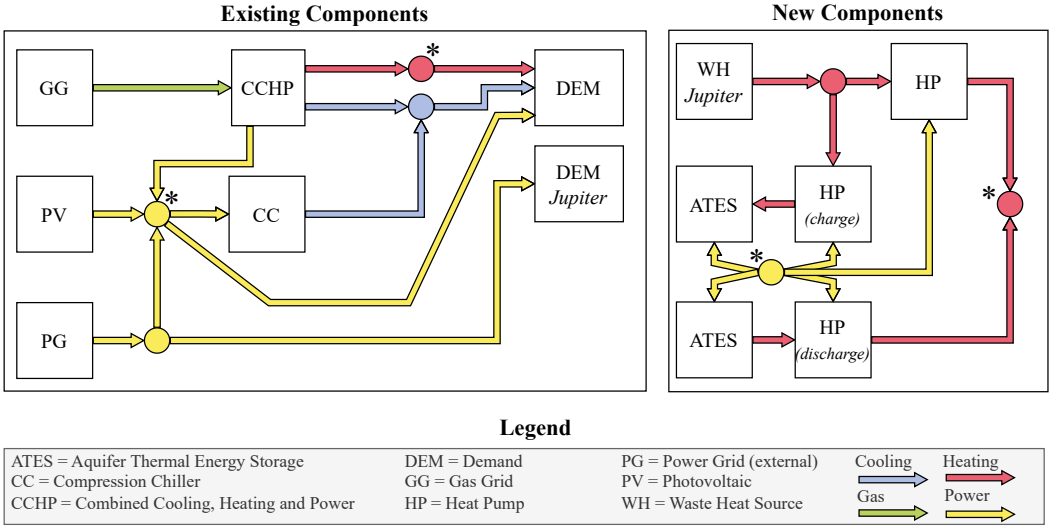

Figure 2. Current and extended energy system of the FZJ. The new components are the WH, HPs and ATES. Note that the nodes in the same colour with * represent the same node for the sake of clarity. Furthermore, the charging and discharging of the ATES cannot occur at the same time.

The PV component was created according to [22]. The electrical power P of this component depends on the solar irradiance in Jülich I, the area of the panels A and the efficiency which was set to $\eta_{PV} = 0.19$. P cannot exceed its nominal capacity P_{nom}=0.171 kW/m^2:

$$P = I \cdot A \cdot \eta_{PV} \tag{6}$$

$$P \leq P_{nom} \cdot A \tag{7}$$

With its estimated area of 8772 m^2, the maximum possible P_{max} is 1.5 MWp.

The DEM component specifies the accumulated heating, cooling and power demand (without *Jupiter*) of the FZJ. The required power demand of *Jupiter* is set constant to the assumed average of 20 MW. It is important to note for the overall energy supply that *Jupiter* have to be supplied by green energy according to the European Green Deal [25]. To ensure that electricity supplied to *Jupiter* does not originate from the CHP plant, a separate green power bus is added to the model. The grid models of the power and gas grid are specified by a steady state consideration of consumption. In addition, the grids are parameterized by the CO_2 factor and the price per consumed commodity, describing emissions and variable costs. The clustered price data, which will be described in Section 3.1, are therefore set as a parameter as well as the fixed parameter for the CO_2 factor of electricity $CO_{2_{el}}$=0 t/MWh[1] and $CO_{2_{gas}}$=0.201 t/MWh [26].

2.2. Extended Energy System

The energy system is extended by the WH, the HP for direct waste heat usage and the HP in combination with the ATES for waste heat storage (Figure 2, right). The WH component describes the waste heat of the *Jupiter* computer with a maximal $\dot{Q}$ of 18 MW. The output temperature is 40 °C and must be increased to between 90 °C and 120 °C using HPs, depending on the flow temperature of the local district heating network. The waste heat can be used directly via the first HP or can be stored in the ATES with the second HP. The second HP, which is partly driven by surplus PV power, increases the temperature up to 80 °C for the storage during the summer. In winter, the HP once again has to elevate the temperature for the district heating network. The capacities of HP and ATES have to be designed. The red arrows in Figure 2 present the thermal power $\dot{Q}$ without consideration of temperatures. To represent the system behaviour, especially of the ATES, the water volume and temperatures have to be considered. Therefore, the energy balance of HP, ATES and WH is based on mass flow $\dot{m}$, temperature difference ΔT and water heat capacity c_p=4.12 kJ/kgK:

$$\dot{Q}_t = \dot{m}_t \cdot c_p \cdot \Delta T_t, \forall t \in \mathcal{T} \tag{8}$$

Note that the product of the variables mass flow $\dot{m}$ and temperature difference ΔT is quadratic which makes the problem quadratically constrained.

2.2.1. Heat Pump Model

The proposed HP model is based on existing work [21,27] and is modified for the use case of this work. The model has one mass flow input $\dot{m}_{evap}$ and output $\dot{m}_{cond}$ and on the evaporator and condenser side the input and output temperatures $T_{evap,in}$, $T_{evap,out}$, $T_{cond,in}$ and $T_{cond,out}$. The thermal power on both sides is expressed by:

$$\dot{Q}_{evap,t} = \dot{m}_{evap,t} \cdot c_p \cdot (T_{evap,in,t} - T_{evap,out,t}), \forall t \in \mathcal{T} \tag{9}$$
$$\dot{Q}_{cond,t} = \dot{m}_{cond,t} \cdot c_p \cdot (T_{cond,out,t} - T_{cond,in,t}), \forall t \in \mathcal{T} \tag{10}$$

As previously shown in Figure 2, the HP has one electrical input. The temperature increase is achieved using electric power P_{el}, which results in the input-output relation:

$$P_{el,t} \cdot T_{cond,out,t} \cdot \eta_{Carnot} \cdot \eta_{pl} = (T_{cond,out,t} - T_{evap,out,t}) \cdot \dot{Q}_{cond,t}, \forall t \in \mathcal{T} \tag{11}$$

[1] In 2024, the FZJ consumed entirely green electricity from the external power grid according to contract.

The part load efficiency η_{pl} is neglected since this would add a non-linear constraint to the model which is still quadratic. The Lorenz approach, which calculates the logarithmic mean temperature of evaporator and condenser, is more precisely for industrial HPs [14,28] but not used here due to the non-linear logarithmic function. Therefore, the Lorenz approach is estimated using the arithmetic mean temperature and η_{Carnot} is replaced by η_{Lorenz} which is set to 0.45 [14]. Note that real-world COP is always limited by irreversibilities, fluid properties, pressure drops and auxiliary energy losses. Furthermore, the energy balance of the HP is set as equality constraint:

$$\dot{Q}_{evap,t} + P_{el,t} = \dot{Q}_{cond,t}, \forall t \in \mathcal{T} \tag{12}$$

The operation is technically constrained by upper and lower limits for $\dot{Q}_{cond}$:

$$\dot{Q}_{min} \cdot b_{op,t} \leq \dot{Q}_{cond,t} \leq \dot{Q}_{design} \cdot b_{op,t}, \forall t \in \mathcal{T} \tag{13}$$

The upper bound is further constrained by the design decision of the HP, where b_{build} is a boolean describing build decision and $\dot{Q}_{max}$ is set to 5.7 MW:

$$\dot{Q}_{design} \leq \dot{Q}_{max} \cdot b_{build} \tag{14}$$

Furthermore, $\dot{Q}_{min}$ depends on the minimum part load λ=20 % [22] and $\dot{Q}_{design}$:

$$\dot{Q}_{min} = \dot{Q}_{design} \cdot \lambda \tag{15}$$

For the cost calculation, it is important to note that the investment costs and specific costs for industrial HPs strongly differs depending on capacity, components, configuration and heat source [29,30]. Therefore, the capacity dependent expression for investment costs I_{HP} (expressed in millions of euros) for excess heat was added to the model [29]:

$$I_{HP} = (0.64114 \cdot \dot{Q}_{design} + 0.29677) \cdot b_{build} \tag{16}$$

2.2.2. ATES Model

The ATES model is developed based on the state of charge (SOC) model proposed by [16]. Since the integration of the ATES in this work focuses on waste heat integration, only the SOC of the hot well $SOC_{ATES,H}$ will be taken into account. Following design decisions have to be made: the nominal capacity E_{design}, the nominal thermal power $\dot{Q}_{design}$ and the boolean b_{build}. The number of well pairs will not be designed and is assumed to one well pair. Additionally, the temperature of the hot well T_H, which charges the ATES, can be designed. Since the installed system should act as an HT-ATES, the bounds for T_H are set from 60 °C to 80 °C. The temperature of the cold well T_C is set as parameter to 35 °C. This value corresponds to the aquifer temperature in Jülich.

The temperature of the hot well is characterized by a periodic change in winter and summer which results in a temperature drop while discharging in winter. This effect makes T_H time dependent since the temperature drop underlies the second law of thermodynamics. However, this thermodynamic behaviour cannot be depicted by energy system optimization models [16]. Therefore and due to the lack of temperature data of the ATES, following restrictions have to be made: A charge and discharge temperature $T_{H,charge}$ and $T_{H,discharge}$ are defined. This restriction has the advantage that $T_{H,charge}$ is now by its

definition time independent and $T_{H,discharge}$ is conservatively set to the fixed value 15 °C below $T_{H,charge}$, representing the assumed maximal loss. The simplified model is shown in Figure 3.

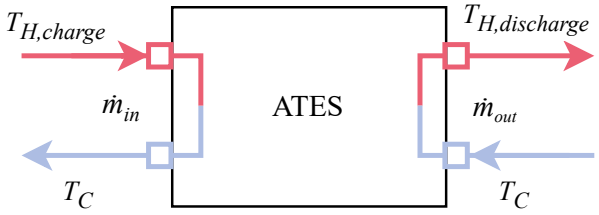

Figure 3. Model of the ATES with $T_{H,charge}$, T_C and $\dot{m}_{in}$ on the charge side. On the discharge side, the model has $T_{H,discharge}$, T_C and $\dot{m}_{out}$. Note that charge and discharge cannot occur at the same time.

Based on these assumptions, the input and output thermal power can be defined as:

$$\dot{Q}_{in,t} = \dot{m}_{in,t} \cdot c_p \cdot (T_{H,charge} - T_C), \forall t \in \mathcal{T} \tag{17}$$

$$\dot{Q}_{out,t} = \dot{m}_{out,t} \cdot c_p \cdot (T_{H,discharge} - T_C), \forall t \in \mathcal{T} \tag{18}$$

The heat flow cannot exceed $\dot{Q}_{design}$ which is restricted to a maximal heat flow $\dot{Q}_{max}$:

$$\dot{Q}_{design} \leq \dot{Q}_{max} \cdot b_{build} \tag{19}$$

Furthermore, the differential equation for the capacity is defined as state variable:

$$E^{ATES,H}_{t+1} = E^{ATES,H}_t + (\dot{Q}_{in,t} - \dot{Q}_{out,t}) \cdot \frac{\tau}{3600} - E^{ATES,H}_t \cdot \sigma^{ATES,H}_t, \forall t \in \mathcal{T} \tag{20}$$

$$\sigma^{ATES,H}_t = \frac{1 - \eta_E}{\Delta t_{heating}} \tag{21}$$

τ describes a time constant for the duration of the charging and discharging which was set to 3600 s according to the hourly clustered data. Note that the product have to be transformed from MWs to MWh and therefore divided by 3600. The ATES cannot be charged and discharged at the same time which is ensured by the logic of the linking component (see Section 2.2.4). $\sigma^{ATES,H}_t$ describes the self-discharge per hour of the ATES with η_E as the thermal recovery efficiency and $\Delta t_{heating}$ the hourly time steps of the heating period in Germany. η_E is set to 80 % and $\Delta t_{heating}$ is set to 5112 (213 × 24 time steps) which represents the heating season from October to April. $E^{ATES,H}_t$ is further constrained by:

$$E^{ATES,H}_t \leq E_{design}, \forall t \in \mathcal{T} \tag{22}$$

$$E_{design} \leq E_{max} \cdot b_{build} \tag{23}$$

Furthermore, it is supposed that the ATES should be at full capacity at the end of September. Thus, the following equality constrained is added to the model where $t_{September}$ is the last timestep referring to September:

$$E^{ATES,H}_{t_{September}} = E_{design} \tag{24}$$

With the assumptions made, the SOC can be defined as:

$$SOC_t^{ATES,H} = \frac{E_t^{ATES,H}}{E_{design}}, \forall t \in \mathcal{T} \tag{25}$$

$$0 \leq SOC_t^{ATES,H} \leq 1 \tag{26}$$

For the pumped groundwater, the electrical power of the water pump can be calculated as:

$$P_{el,t} = \frac{g \cdot h \cdot \dot{m}_t}{\eta_p}, \forall t \in \mathcal{T} \tag{27}$$

Where g is the gravity factor, h the depth of the aquifer layer, $\dot{m}_t$ the mass flow and η_p the water pump efficiency of 68 %. As stated before, the in and out mass flow $\dot{m}_{in,t}$ and $\dot{m}_{out,t}$ cannot occur at the same time. The operational costs are determined by the power consumption of the water pumps. The operational costs of the HP are not part of the ATES model. They are considered separately in the HP model. The investment costs are calculated in simplified manor dependent on the designed $\dot{Q}_{design}$ and specific costs C_{spec}:

$$I_{ATES} = C_{spec} \cdot \dot{Q}_{design} \cdot b_{build} \tag{28}$$

As the performance depends on local conditions, the maximum values are set according to the values calculated in the preliminary feasibility study (Table 1).

Table 1. Maximal values of the investigated parameters for the ATES

Parameter	Value
E_{max}	25 000 MWh
$\dot{Q}_{max}$	13 MW
$\dot{m}_{max}$	82 kg/s
$P_{el,max}$	0.25 MW
C_{spec}	10^6 €/MW

2.2.3. Waste Heat Source Model

The WH model depicts the waste heat of the *Jupiter* computer. The nominal $\dot{Q}_{max}$ of the WH is set to 18 MW. The input temperature is set to 30 °C and the output temperature is 40 °C. The waste heat profile is well suited for district heating since its stable supply flow [31]. Due to this fact, the temperatures are approximated to fixed values. Assuming temperatures as fixed parameters makes the expression for the thermal power $\dot{Q}_{WH}$ linear:

$$\dot{Q}_{WH,t} = \dot{m}_{WH,t} \cdot c_p \cdot (T_{WH,out} - T_{WH,in}), \forall t \in \mathcal{T} \tag{29}$$

The thermal power is constrained to:

$$\dot{Q}_{WH,t} \leq \dot{Q}_{max}, \forall t \in \mathcal{T} \tag{30}$$

For the sake of simplicity, no investment costs and specific costs were assumed. Consequently, the expenditures associated with supplementary installations for waste heat recovery were not considered.

2.2.4. Linking Component

The linking component does not represent a physical component to be installed in the energy system. It is basically a subsystem of COMANDO's *System* class which ensures the switch between the charging and discharging of the ATES. As shown in Figure 4, the linking component consists of the same HP in different operational modes charge and discharge, which will be denoted by HP^{ch}_{ATES} and HP^{dis}_{ATES} in the following. These modes are implemented by two HP objects. The evaporator input temperature $T_{evap,in}$ of HP^{ch}_{ATES} is the output temperature $T_{WH,out}$ of the WH. HP^{ch}_{ATES} raises this temperature up to $T_{H,charge}$ and charges the hot well of the ATES. The input temperature on the condenser side $T_{cond,in}$ is the groundwater temperature of the cold well. In the discharge mode, HP^{dis}_{ATES} takes $T_{H,discharge}$ on the evaporator side and raises this temperature to the required district heating network temperature between 90 °C and 120 °C on the condenser side. The evaporator return temperature $T_{evap,out}$ corresponds to the cold well temperature.

To ensure that the ATES cannot be charged and discharged at the same time, the following constraint is added to the model:

$$b_{ch,t} + b_{dis,t} \leq 1, \forall t \in \mathcal{T} \tag{31}$$

Since the subsystem contains the same HP, it must be ensured that $\dot{Q}_{design}$ is the same for both HP objects. This is guaranteed by:

$$\dot{Q}^{HP^{ch}_{ATES}}_{design} = \dot{Q}^{HP^{dis}_{ATES}}_{design} \tag{32}$$

The investment costs for the two HP objects were halved to represent one full physical HP. Because of the abstract nature of the linking component, no costs are associated with it.

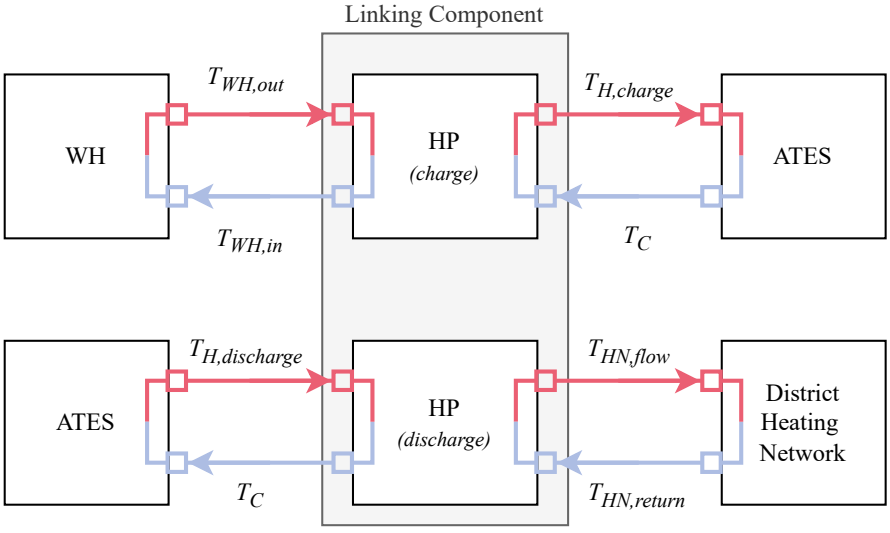

Figure 4. Linking component with the same HP at different operation modes: In charge mode, the ATES is charged by the HP with waste heat from the *Jupiter* computer. In discharge mode, the ATES is discharged and the HP feeds into the district heating network.

2.3. Objectives

In this work the TAC and the GWI are optimized as a bi-objective optimization problem. The TAC comprises capital expenditures (CAPEX), reflecting the investment costs, and operational expenditures (OPEX), which describe operational costs depending

on electricity and gas consumption. Additionally, fixed costs like maintenance costs are included. Therefore, the TAC is calculated by:

$$TAC = \frac{(1+i)^{n \cdot i}}{(1+i)^n - 1} \cdot \sum_{j \in \mathcal{N}} CAPEX_j + \sum_{k \in \mathcal{U}} \gamma_k \cdot CAPEX_k + OPEX \tag{33}$$

Where i is the assumed interest rate of 1.2 % [32] and n the considered time horizon of 20 years [23]. The investment costs of the additional components $j \in \mathcal{N}\{ATES, HP\}$ have to be amortized over the set time horizon. The costs of the already existing components $k \in \mathcal{U}\{B, CHP, AC, CC, PV\}$ are considered as maintenance costs with a specific maintenance coefficient γ_k (see Appendix A1). Note that costs for peripheral components like pipes, transformers, grid connection points or control systems are not considered. The OPEX are the cumulative costs for electricity $P_{el,t}$ and gas $\dot{Q}_{gas,t}$ and are weighted by the number of time steps w_t corresponding to the time horizon $\mathcal{T}$:

$$OPEX = \sum_{t \in \mathcal{T}} w_t \cdot (C_{el,t} \cdot P_{el,t} + C_{gas,t} \cdot \dot{Q}_{gas,t}) \tag{34}$$

The GWI as the other objective function is calculated by the CO_2 factor of electricity and gas and depends on the consumed $P_{el,t}$ and $\dot{Q}_{gas,t}$. As the OPEX, the GWI is also weighted by w_t:

$$GWI = \sum_{t \in \mathcal{T}} w_t \cdot (CO_{2_{el}} \cdot P_{el,t} + CO_{2_{gas}} \cdot \dot{Q}_{gas,t}) \tag{35}$$

With the quadratic constraints (17), (18) and the objective functions, the optimization problem is of type MIQCP.

3. Case Studies

The developed energy system optimization model enables the investigation of various use cases, facilitating the assessment of the economic and ecological performance of the entire system with the HT-ATES. Therefore, demand and price data of the FZJ are firstly described as parameters for the optimization model. After that, a brief overview of the case studies and sensitivity analyses are presented as well as methods for solving the case studies optimization problem. The current energy system of the FZJ (Figure 2, left) is regarded as the reference case. In this scenario, the waste heat of *Jupiter* is not utilized, however, its power demand of 20 MW must be met.

3.1. Data Preparation

Data is prepared to define the specific values of the parameters for optimization. Therefore, time-series of price and demand data in 2024 are preprocessed and clustered with the Python packages *numpy*, *pandas* and *sklearn*. The datasets are resampled to hourly mean values to save computational resources, with data falling outside the 1.5 interquartile range excluded and missing values interpolated. These outliers are only excluded in the demand data due to inaccurate sensor measurement. Price data are not adjusted for outliers since spot market prices can fluctuate in high ranges due to special events.

Price data include the electricity and gas prices according to the spot market as shown in Figure 5. The electricity price is fluctuating between -10 and 2300 €/MWh. The high peak of 2300 €/MWh was due to technical problems at the European Power Exchange (EPEX) spot market that affected the market balance. The average electricity price in 2024 is 79.51 €/MWh. The gas price is more stable than the electricity price and fluctuates in the range of 25 to 50 €/MWh. The trend shows an increase throughout the year with an average price of 34.61 €/MWh.

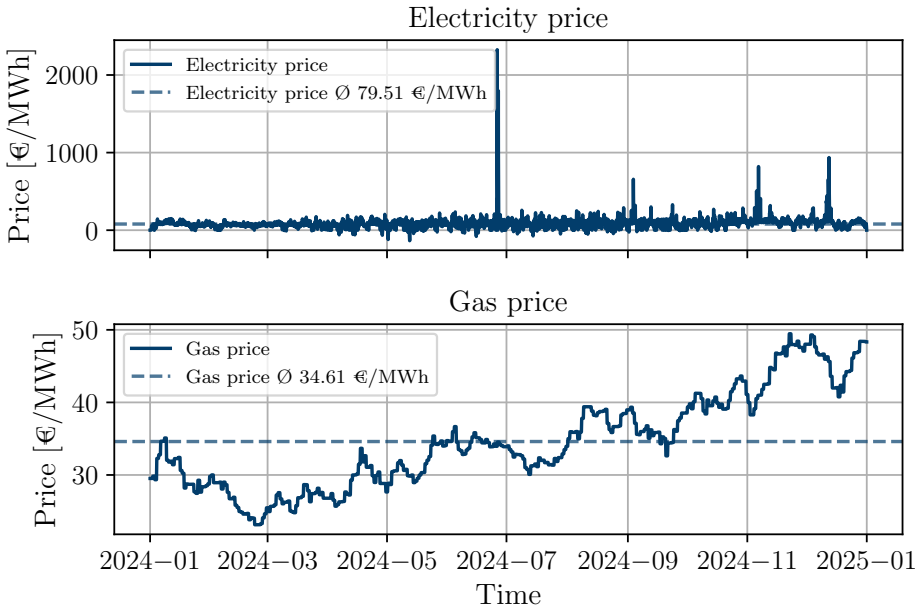

Figure 5. Electricity and gas prices based on the contract of the FZJ for the consumed commodities in 2024.

Demand data consist of heating, cooling and power demand of all FZJ buildings as presented in Figure 6. The heating demand, which varies between 10 and 30 MW in winter and values around 4 MW in summer, is in typical range of a small town. The peak reaches values up to 36 MW. The flow temperature of the heating network is between 90 °C and 120 °C while the return temperature is around 60 °C. The cooling demand varies below 4 MW in the winter months and reaches values up 7 MW in summer. The average cooling demand is 4.63 MW. The power demand consists of electricity, which is produced by the gas-fired CCHP plant at FZJ and electricity, which is supplied by the external power grid. It is important to emphasize that the electricity supplied by the power grid in 2024 is entirely renewable, as contracted, and therefore emission-free. The power demand has an average value of 11.51 MW.

In total, the preprocessed data consist of 8784 (366×24) time steps and nine features: heating, cooling and power demand, solar irradiance, flow and return temperature of the heating network, ambient temperature and gas and electricity price. To save computational resources, a clustering algorithm is implemented. The algorithm is based on *sklearn* k-means clustering algorithm and is performed for each month to save the time coupling between the data points. This is important for the evaluation of the ATES operation in a seasonal manner. Via the silhouette-score, an optimal number of two cluster points for each month was determined which results in 24 cluster centers.

To assign the discretized time horizon $\mathcal{T}$, the number of data points corresponding to each cluster center is determined. In addition to the cluster centers, the peak demands, temperatures and prices have to be taken into account. The peak values have no effect on the objective but are necessary for feasibility of the system [21]. This is ensured by setting the corresponding time step to zero. The detailed clustered dataset with peak values, months and timesteps can be found in Appendix B1.

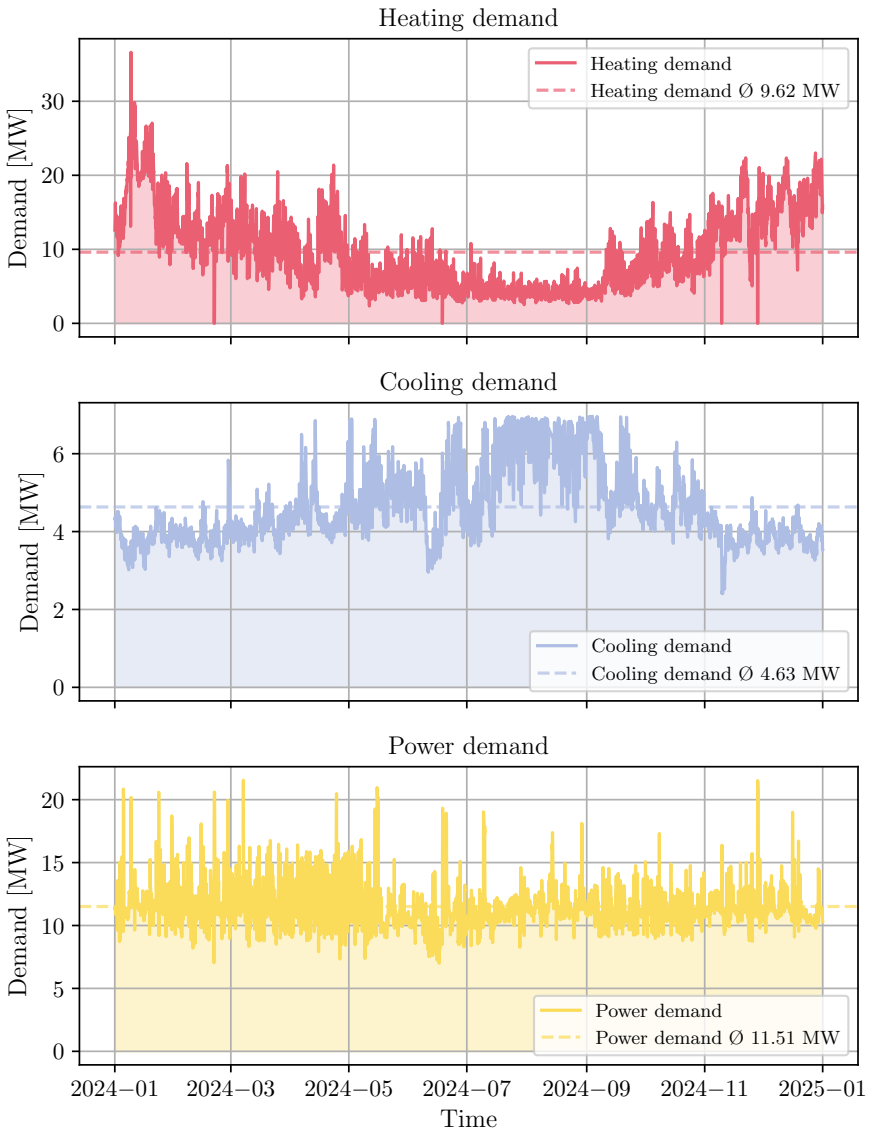

Figure 6. Heating, cooling and power demand of the FZJ in 2024.

3.2. Overview and Solution of the Case Studies

According to Table 2, a brief overview of the case studies and sensitivity analyses is provided: The first case study (CS_I) focuses on the extended energy system, which incorporates the novel components WH, HPs, and HT-ATES into the existing system. The design and optimization of the new components must be executed simultaneously. In the second case study (CS_{II}), the extended system without the CCHP is investigated. Therefore, the CCHP is replaced by two boilers with $\dot{Q}_{max}$ of 16 MW and $\dot{Q}_{max}$ of the HPs is increased to 11.4 MW. It is essential that the investigation addresses how the heating demand can be satisfied primarily by waste heat, HPs and HT-ATES. Finally, the sensitivity analyses (S_I and S_{II}) evaluate the influence of a reduced temperature loss in the HT-ATES and energy prices on the system behaviour. Both are conducted with the extended energy system of CS_I. S_I analyzes the impact of a 10 °C decrease in temperature of the hot well on the design variables of the extended energy system. It has been demonstrated that a stabilized well temperature during several years of continuous operation will result in a reduced temperature loss [33]. S_{II} investigates the influence of changed electricity and gas prices with an increase of 10 % and 50 %, respectively. Due to the uncertain nature of future gas and electricity prices, these costs are expected to influence system design and operation.

Table 2. Overview of the case studies and sensitivity analyses

Case study	**Description**
Ref	Reference system
CS_I	Extended energy system
CS_{II}	System without CCHP
Sensitivity analysis	**Description**
S_I	HT-ATES with 10 °C temperature loss
S_{II}	Electricity price + 10 %; gas price + 50 %

For the solution of the case studies optimization problem, the algebraic modeling language (AML) Pyomo 6.9.2 and the solver Gurobi 12.0.0 are used. Gurobi uses a combination of various algorithms for optimization like branch and bound, relaxation or cutting planes. Furthermore, the non-convex optimization flag is set with 0 % optimality gap. All results were obtained in a few seconds of CPU time. With the increased prices, the computing time rose by eight seconds compared to the default prices. The ε-constraint routine, which alternates between TAC and GWI optimization, identifies six Pareto optimal solutions. All case studies are performed on a PC with an i7-1365U CPU (1.80 GHz), 32 GB RAM, running Windows 11 Enterprise.

4. Results

In this chapter, the results of the reference system (Ref), the two case studies (CS_I, CS_{II}) and the sensitivity analyses (S_I, S_{II}) are presented. The bi-objective optimization results are displayed as Pareto fronts. The Pareto front can be interpreted as such: solution 1 is the most expensive with the lowest GHG emissions, whereas solution 6 is the least expensive with the highest GHG emissions. Additionally, the HT-ATES operation is evaluated on a seasonal basis and the corresponding design values of the HT-ATES are presented. The term ATES is used to refer to HT-ATES in the following.

4.1. Reference Energy System

The current energy system at FZJ is composed of existing components that do not utilize and store *Jupiter* waste heat. The low-temperature district heating network as investigated in [34] and [35] was not taken into account in this study. Figure 7 presents the Pareto front as a stacked bar chart of system components. The annual outputs are calculated by summing the monthly outputs. The orange bars in the graph represent the combined output of the three CHP units, which includes electricity and heat. The red bars, on the other hand, indicate the output of the two boilers.

The TAC ranges from 23.26 to 24.78 Mio. €/a, and the GWI ranges from 36.72 to 47.72 kt_{CO_2}/a. As previously mentioned in Section 2.1, the stable operation of the CCHP is ensured by the AC, which absorbs the surplus heat and provides cooling capacity. This indicates that a decline in CHP heat output (from 194 to 128 GWh) is accompanied by a reduction in AC output (from 19.04 to 8.84 GWh). The deficit in cooling capacity is then provided by the CC (from 21.65 to 31.85 GWh). The reduced heat output, resulting from a reduction in CHP operation, is compensated by increased boiler output (from 11.14 to 26.84 GWh). The findings indicate that the current system is predominantly characterized by the combined heat and power generation of gas-fired CHP plants. A decrease in CHP heat output means more electricity must be purchased from the external power grid at higher prices. Overall, these related effects make the system more expensive but they also reduce the GWI. This is because less gas is used and the electricity is purchased as green electricity from the grid.

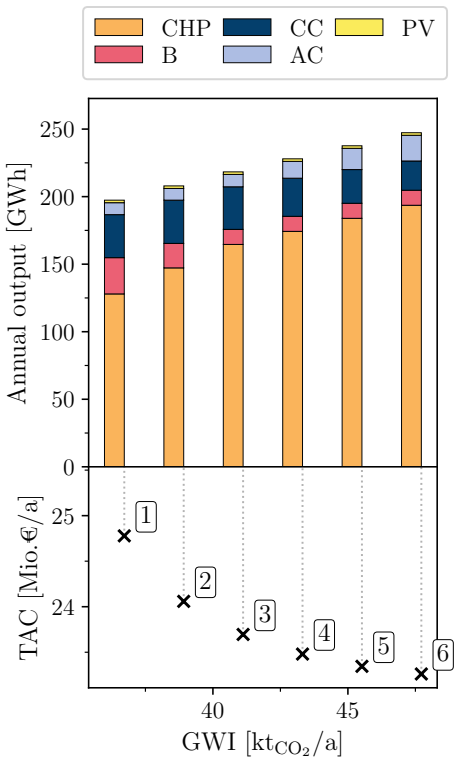

Figure 7. Pareto front of the current energy system (Ref).

4.2. Case Study I and II: Extended and Future Energy System

Figure 8 (a) shows the results of the case study CS_I, which includes the additional components HP_{WH}, HP^{ch}_{ATES}, HP^{dis}_{ATES}. Note that the right y-axis refers to the installed nominal thermal power of the additional components, denoted by striped bars. These bars represent the results of the design optimization. The HP_{ATES} indicates the nominal thermal power of HP^{ch}_{ATES} and HP^{dis}_{ATES}, as it operates in both modes. The minimum TAC is 23.16 Mio. €/a with a GWI of 47.80 kt_{CO_2}/a (solution 6). The minimum GWI is 29.47 kt_{CO_2}/a with a TAC of 25.05 Mio. €/a (solution 1). While the minimum TAC is comparable to Ref, the GWI is reduced by 7.25 kt_{CO_2}/a in solution 1. This equates to a 20 % reduction compared to Ref, yet costs only increase by 1 %. While the CHP operation is similar to Ref, the boiler usage decreases (from 6.14 to 1.24 GWh) due to an increase in the direct usage of waste heat (from 3.38 to 21.2 GWh). Consequently, the designed power of HP_{WH} also increases (from 1.23 to 5.7 MW). The designed HP_{ATES} power is negligible for Pareto solution 2 to 6. The HP_{ATES} in conjunction with the ATES is only build and used in the least emission but most expensive case. For solution 1, HP_{ATES} is designed to 5.23 MW. The HP^{dis}_{ATES} has an annual output of 6.71 GWh, whereas the HP^{ch}_{ATES} has an output of 6.13 GWh. This results in a minimum GWI of 29.47 kt_{CO_2}/a.

Figure 8 (b) illustrates the Pareto front of CS_{II}. The minimum TAC is 25.75 Mio. €/a with a GWI of 7.86 kt_{CO_2}/a. The GWI is minimized to 3.18 kt_{CO_2}/a, with TAC of 26.28 Mio. €/a. This results in a 91 % GWI reduction, accompanied by a 6 % increase in TAC compared to Ref. The boiler output decreases (from 31.29 to 12.65 GWh), while the CC output stays at 40.69 GWh since it is the own cooling supplier. The HP_{WH} output remains between 46.91 GWh (solution 6) and 44.59 GWh (solution 1) with an installed power of 6.10 MW for solution 1. This illustrates that direct waste heat utilization is the primary heat source due to its constant annual output and power. The ATES with the HP_{ATES} is built and used in all Pareto solutions, in contrast to CS_I. Therefore, it can be posited that the ATES system is a necessary component for future applications aimed at reducing emissions: The

usage of HP^{ch}_{ATES} increases (from 5.40 to 23.92 GWh) and HP^{dis}_{ATES} (from 6.26 to 27.22 GWh). The newly installed power increases for the HP_{ATES} from solution 6 to 1 (from 1.56 to 10.74 MW). The more boiler output is replaced by the HP_{ATES}, the lower the system's emissions. Nonetheless, due to the absence of the CCHP, the full electricity demand is supplied by the external power grid. In conjunction with the augmented nominal thermal power of HPs and ATES, this results in higher overall TAC compared to Ref and CS_I. In this particular scenario, the only fossil source is the boiler which is only used during periods of peak demands. The utilization of HPs and ATES is predominant and the incorporation of green electricity from the power grid leads to a marginal GWI.

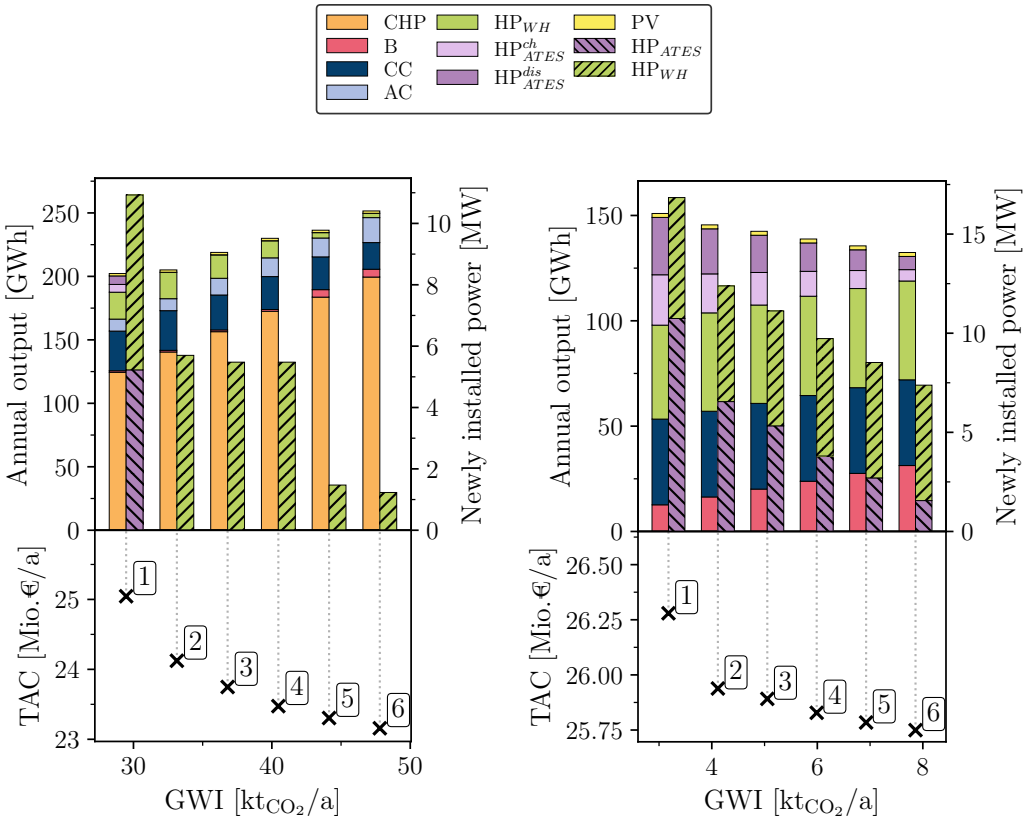

(a) (b)

Figure 8. (a): Pareto front of the extended energy system (CS_I).(b): Pareto front of the extended system without CCHP (CS_{II}). Note that the right y-axis refers to the installed nominal power of the additional components, denoted by striped bars. The left y-axis corresponds to the non-striped bars.

4.3. Case Study I and II: ATES Operation and Design

Figure 9 shows the SOC (red bars) of the ATES for CS_I. Since the ATES is only build for Pareto solution 1, this result will be further analysed. The light blue bars represent the discharge mode (b_{dis}) and the light red bars the charge mode (b_{ch}) of the HP_{ATES}. The dotted black curve displays the electricity prices (C_{el}). E_{design} is 5134 MWh, which is 21 % of the maximum possible ground capacity. From January to March the ATES is mainly discharged, except one cluster point in February where the electricity price drops to 60 €/MWh and the ATES is charged at 13 %. This emphasizes the ATES flexibility even during winter charging. However, this would be only possible when the price and the heating demand are low. Until March, the ATES is discharged to 5 %. From April onwards, the ATES is charged in steps, attaining full capacity by September. The HP_{ATES} operates in charge mode during summer periods when the electricity price is low, thereby ensuring an economic operation. The SOC loss during summer in the white periods is due to the

self-discharge. After reaching full capacity in September, the HP_{ATES} switches to discharge mode at the final four cluster points. By the end of the year, the SOC of the ATES is expected to reach 37 %. This operation demonstrates a low emission heat storage utilization that is favorable in the winter months.

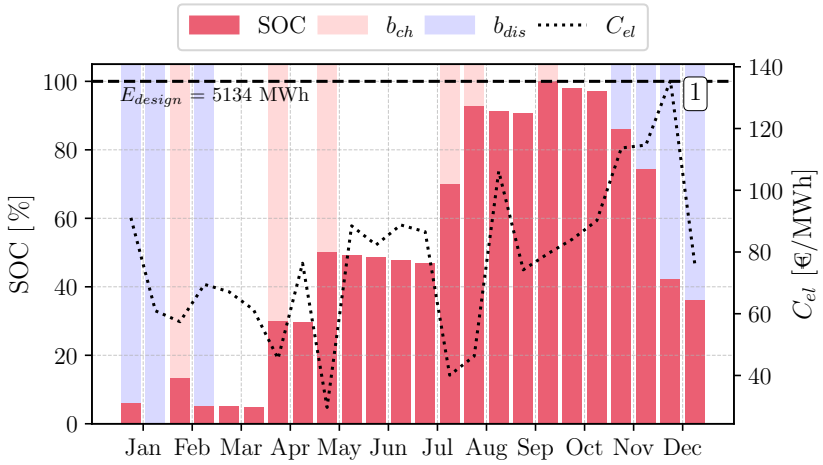

Figure 9. SOC of ATES for CS_I

Figure 10 shows the SOC (red bars) of the ATES for CS_{II}. Given the similarity of the operation for the ATES for the six solutions, only solution 1 is analyzed as an example of the most ecologically design and operation. The capacity is designed to 16 990 MWh, which equates to 68 % of the ground's maximal possible capacity. This clearly demonstrates a more preferable storage usage compared to CS_I. At the beginning of the year, the SOC is at 25 % and similar to CS_I, the ATES is charged in February due to a decline in the electricity price. In addition, the ATES demonstrated its flexible operation in April, when the SOC reduces from 18 % to 5 % due to discharging. From May to September, the ATES is charged regardless of the electricity price to reach full capacity in September. This is due to the reduced degrees of freedom of the MIQCP, as the CCHP was excluded. Given the considerable proportion of the heat supply in this system that is accounted by the ATES, it is discharged continuously during the winter periods, reaching 43 % by the end of the year.

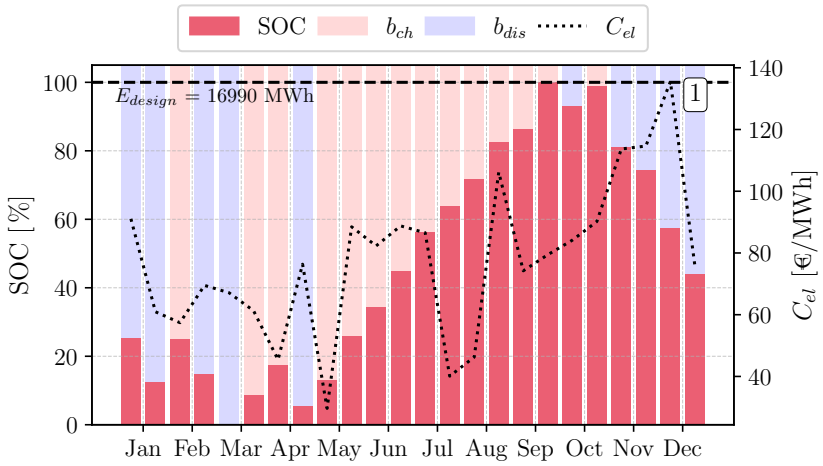

Figure 10. SOC of ATES for CS_{II}

Table 3 provides a short overview of the design variables for CS_I compared to CS_{II}, especially for the ATES system. For CS_I, $T_{H,charge}$ is designed to 80 °C which is the maximum possible design temperature for the given problem. $T_{H,discharge}$ is designed to 65 °C due to

the assumed fixed loss of 15 °C. The $\dot{Q}_{ATES}$ was designed to 4.01 MW. With the $\dot{Q}_{HP_{ATES}}$ of 5.23 MW, this results in an estimated COP of 4.29 for the HP_{ATES} at full load during discharging.

For CS_{II}, $T_{H,charge}$ is designed to 75 °C which is 5 °C lower than CS_I. $T_{H,discharge}$ is designed to 60 °C. With the designed ATES power of 8.08 MW and HP_{ATES} power of 10.74 MW, the estimated COP is 4.04 at full load of discharging. The COP is lower than CS_I due to the lower discharge temperature, which increases the difference to the flow temperature of the district heating network.

Table 3. Design values of the first Pareto solution for CS_I and CS_{II}

Design variable	**CS_I**	**CS_{II}**
$\dot{Q}_{ATES}$	4.01 MW	8.08 MW
$T_{H,charge}$	80 °C	75 °C
$T_{H,discharge}$	65 °C	60 °C
E_{ATES}	5134 MWh	16 990 MWh
$\dot{Q}_{HP_{ATES}}$	5.23 MW	10.74 MW
$COP_{HP^{dis}_{ATES}}$	4.29	4.04
TAC	25.05 Mio.€/a	26.28 Mio.€/a
GWI	29.47 kt_{CO_2}/a	3.18 kt_{CO_2}/a

4.4. Sensitivity Analysis I: Reduced Temperature Loss

S_I investigates the influence of a reduced temperature loss of 10 °C in the hot well on the design variables of the ATES. The temperature loss was estimated based on [33]. It should provide a rough estimation of the future design and operation with a stabilized temperature in the hot well after a few years of continuous operation. Since the Pareto fronts are similar, only the ATES design values of the first Pareto solution are presented and compared here. Table 4 shows the results of the first Pareto solution for S_I (ΔT=10 °C) compared to CS_I (ΔT=15 °C). A reduced temperature loss of 10 °C in the hot well results in a higher $\dot{Q}_{ATES}$ of 4.09 MW. The estimated COP at full load for the HP^{dis}_{ATES} is 4.29 in CS_I and 4.59 in S_I. $T_{H,charge}$ is 80 °C for both solutions but consequently S_I has a $T_{H,discharge}$ of 70 °C. E_{design} is also increased to 6825 MWh which is 27 % of the maximum possible capacity. $\dot{Q}_{HP_{ATES}}$ remains the same with 5.23 MW. The reduced temperature loss also yields a slightly reduced TAC of 25.04 Mio. €/a, compared to 25.05 Mio. €/a. Therefore, the TAC could be reduced in future with a higher HP efficiency due to a stabilized hot well temperature. The GWI remains at 29.47 kt_{CO_2}/a, showing that reduced temperature loss does not affect the system's overall emissions.

Table 4. Design values of the first Pareto solution for S_I compared to CS_I

Design variable	**S_I: ΔT=10 °C**	**CS_I: ΔT=15 °C**
$\dot{Q}_{ATES}$	4.09 MW	4.01 MW
$T_{H,charge}$	80 °C	80 °C
$T_{H,discharge}$	70 °C	65 °C
E_{ATES}	6825 MWh	5134 MWh
$\dot{Q}_{HP_{ATES}}$	5.23 MW	5.23 MW
$COP_{HP^{dis}_{ATES}}$	4.59	4.29
TAC	25.04 Mio.€/a	25.05 Mio.€/a
GWI	29.47 kt_{CO_2}/a	29.47 kt_{CO_2}/a

4.5. Sensitivity Analysis II: Increased Energy Prices

In this sensitivity analysis, the electricity price is increased by 10 % while the gas price is increased by 50 %. Changed energy prices are a potential uncertainty that could occur in the future. Figure 11 (a) shows the Pareto front of S_{II} for increased energy prices. The Pareto front of CS_I with default energy prices is presented in (b), which is the same plot as Figure 8 (a). For S_{II}, the TAC is minimized to 28.55 Mio. €/a with a GWI of 39.82 kt_{CO_2}/a. The GWI is 7.98 kt_{CO_2}/a lower compared to the default prices and the TAC is 5.39 Mio. €/a higher. The GWI is minimized to 29.47 kt_{CO_2}/a, similar to CS_I, with TAC of 29.46 Mio. €/a, which is 18 % higher than in CS_I. Since there is no difference in GWI for solution 1, it indicates that the system cannot be designed or operated in a more ecological manner, which is important for robust ecological system design. The main differences are reduced boiler and CHP operation, as well as increased HP_{WH} installed nominal power and operation, especially for the right Pareto solutions. The output of gas-driven components, such as CHP and boilers, is particularly affected by the higher increase in gas price compared to electricity price. The boiler output decreases (from 1.39 to 1.24 GWh) and the CHP output also decreases (from 169.7 to 124.4 GWh). This reduction necessitates the direct waste heat integration to cover the heat demand. Consequently, this results in a higher installed nominal power and output of the HP_{WH}. The HP_{WH} output increases (from 13.72 to 21.2 GWh). The installed nominal power for HP_{WH} range from 5.48 MW (solution 6) to 5.7 MW (solution 1). With focus on the ATES and the HP_{ATES}, they are also installed for the second Pareto solution, besides the first solution. In essence, the system's overall cost rises due to increased energy prices, yet the significance of HPs and ATES for achieving a balanced economic and ecological system design is amplified.

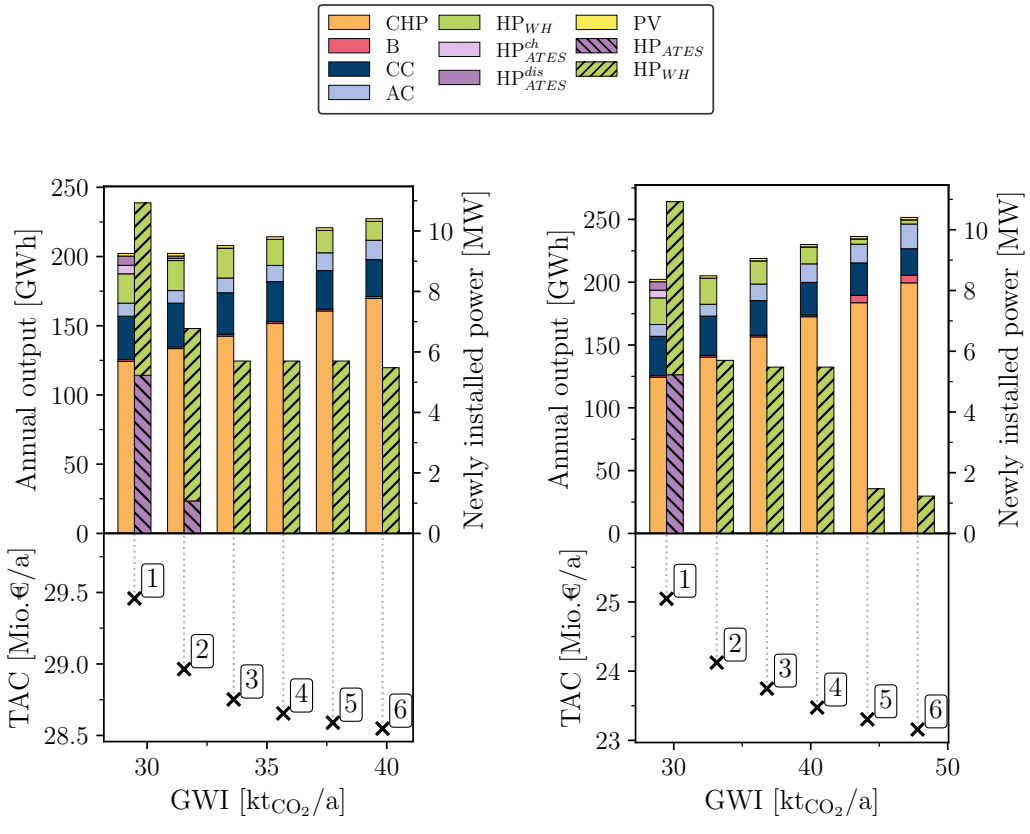

Figure 11. (a): Pareto front for increased energy prices (S_{II}). (b): Pareto front for default prices (CS_I). Note that the right y-axis refers to the installed nominal power of the additional components, denoted by striped bars. The left y-axis corresponds to the non-striped bars.

5. Discussion

In this section, the results for the two case studies and sensitivity analyses are discussed from an economic and ecological perspective. This discussion aims to evaluate the HT-ATES potential for the investigated energy system. It is essential to acknowledge the limitations inherent in the model assumptions and the generalizability of the results.

CS_I reveals the emission reduced potential of the ATES, already in the existing energy system of FZJ. The ATES is only installed in the most expensive, lowest-emission scenario. This results in a 20 % emission reduction compared to Ref, with a 1 % increase in TAC. As previously mentioned, the incorporation of the ATES and HP as new components has a substantial impact on the operation of the existing components. Therefore, direct waste heat utilization and waste heat storage reduce boiler and CHP production. The operational optimization indicates that the ATES increases the system's degree of freedom, allowing flexible, market price-dependent operation. At times of low electricity prices, the ATES is charged, which is economically sensible given that the HP requires large amounts of electricity to maintain a temperature raise from 40 °C to 80 °C. Similar, as analyzed in [17] with a MILP approach, reduction of costs and emission cannot be reached in the simultaneously through the integration of the ATES. As indicated in [17], the HPs have been identified as a primary factor contributing to the overall costs. In this context, the HP_{WH} has to raise the temperature only once for the direct integration into the heating network. Conversely, the HP_{ATES} is required to raise the temperature during both the charging and discharging processes, in addition to compensating for temperature losses. During discharging, this increase is smaller, but HP_{ATES} requires more electricity than direct waste heat utilization. Furthermore, the utilization of surplus PV electricity during summer months could enhance the cost-efficiency of the HP_{ATES}.

CS_{II} demonstrates that in a possible long-term scenario without CCHP, in which the electricity demand is fully supplied by the grid as renewable power and with boilers serving as the sole fossil fuel source, ATES and HPs are crucial for achieving substantial emission reductions. However, it should be noted that the GWI is already in a low range, compared to Ref, due to the set parameters of this particular scenario and the zero CO_2-factor of the consumed electricity. Therefore, the GWI can be reduced by 91 %, accompanied by a 6 % increase in TAC compared to Ref. The necessity of ATES is further emphasized by the improved capacity and performance. The lower charging and discharging temperatures are also noteworthy, as they result in a slight reduction in the COP of the HP_{ATES}. However, the injection temperature of the hot well has been identified as a key ATES parameter: lower injection temperatures can improve recovery efficiency [36]. Due to thermal conduction, this effect was not taken into account by the developed optimization problem and thus neglected assuming a constant recovery efficiency. Nevertheless, this aspect of the lower charging temperature should be mentioned. Operational optimization demonstrates a summer charging phase that is less flexible, as the higher capacity necessitates continuous charging throughout the summer months. This is disadvantageous, as the high power consumption of the HP increases the TAC. This phenomenon may be counterbalanced by the augmentation of PV facilities. As the ATES have the potential to enhance the renewable energy penetration level [16], it can be posited that an optimal synergy between PV and the ATES could be achieved.

The reduced temperature loss in S_I leads to an increase in both the ATES power and the capacity, consequently resulting in a decrease in TAC. Important to mention is that this work only focuses on a one year optimization and can therefore only make limited conclusions about long-term effects on costs. However, it has been shown that the ATES can reduce the levelized cost of heat in the long-term [33].

S_{II} shows the increasing importance of ATES and HP at higher relative fossil gas prices compared to electricity. It must be acknowledged that this is a hypothetical assumption. Nevertheless, prices are a crucial parameter that can exert a substantial influence on the target variable and, consequently, on the outcome of the design and operation. In this case the higher prices result in an increase in TAC of 18 % compared to the normal prices. Notwithstanding, the Pareto solution with the minimal emissions, exhibits stability in the context of price fluctuations.

The model under consideration is subject to certain limitations with regard to the assumptions made. The results depend on the specified maximum permissible values for thermal power or mass flow. The values of the design variables and the operational parameters will be subject to variation. Consequently, the findings cannot be generalized to other energy systems with HT-ATES, particularly with respect to the zero CO_2-factor of the consumed electricity. The specific ATES investment costs are also based on simplified estimations and may differ from the actual results in the future. Additionally, the assumed fixed temperature loss and temperature levels are approximate estimations. The implementation of a time-dependent temperature simulation, incorporating a designated time row as a parameter, could serve as a valuable extension. Furthermore, the HP efficiency could be enhanced by reducing the flow temperature of the district heating network. Since the potential of the ATES was not fully exploited in all case studies, it would be conceivable to supply additional consumers with the stored waste heat. For instance, the direct utilization of stored waste heat via a heat exchanger could be investigated. Therefore, an additional heating demand with the same temperature level could be connected to the ATES. Moreover, the operational dynamics of the district heating network incorporating an HT-ATES could be simulated.

6. Conclusions

The aim of this study was to optimize an existing energy system with an HT-ATES charged by renewable HPC waste heat. Therefore, the operation and design of the system was optimized with a MIQCP approach in economic and ecological terms for different use cases.

The emission-reduction potential of the HT-ATES for the investigated energy system becomes particularly evident in individual applications. Initially, the HT-ATES was integrated into the existing energy system in CS_I. In this instance, emissions can be reduced by 20 % while costs increase by 1 % compared to the reference system, including the integration of HT-ATES. The operational optimization exhibited an economic charging pattern during the summer months. The design of a potential idealized future system, as investigated in CS_{II}, can be accomplished through the implementation of HT-ATES, HPs and waste heat as the primary heat supply. The HT-ATES integration can reduce emissions by up to 91 % while increasing costs by 6 % compared to the reference system. However, the HT-ATES charging method during summer months is less economic due to its high capacity. In addition, the sensitivity analyses S_I and S_{II} demonstrated the dependence of the results on the assumed hot well temperature loss and energy prices. Therefore, a small reduction in TAC of 0.01 Mio.€/a could be expected in the future as well as an increased importance of HT-ATES and HPs for higher gas prices.

A comprehensive analysis of the examined scenarios reveals the considerable potential of the HT-ATES and HPs in conjunction with the renewable HPC waste heat. The HT-ATES is designed and operated in a flexible manner within the overall system. Furthermore, the necessity of HT-ATES in the existing system to achieve minimum GWI has been demonstrated. The TAC is particularly influenced by the design and operation of the HPs and the HT-ATES. Several model improvements could be made for future applications. For

instance, simulations could be conducted to study the well temperature under different operating strategies. Additionally, more consumers could be integrated into the energy system and supplied by the HT-ATES due to its high capacity. Furthermore, the entire district heating network with the HT-ATES integration could be simulated.

Author Contributions: Conceptualization: N.H.; methodology: N.H.; software: N.H.; investigation: N.H.; writing—original draft preparation: N.H. and A.X.; writing—review and editing: N.H., A.X. and D.M.; visualization: N.H. and A.X.; supervision: A.X. and D.M.; project administration: A.X.; All authors have read and agreed to the published version of the manuscript.

Funding: This research received no external funding.

Data Availability Statement: The data presented in this study are currently not publicly available. The publication of anonymized and aggregated data is in preparation.

Acknowledgments: The authors gratefully acknowledge the cooperation with the project partners in FZJ (especially Intelligent Campus, Facility Management, Building Department, Jülich Supercomputing Center, IT Services). Moreover, the work of the related staff at ICE-1 supporting and enabling the project is greatly appreciated. The authors would also like to express their particular gratitude to the Deep Geothermal Energy and Borehole Systems department at Fraunhofer IEG.

Conflicts of Interest: The authors declare no conflicts of interest.

Nomenclature

Abbreviations and Component Labels

AI	Artificial Intelligence
AML	Algebraic Modeling Language
ATES	Aquifer Thermal Energy Storage
CAPEX	Capital Expenditures
CC	Compression Chiller
CCHP	Combined Cooling, Heating and Power
CHP	Combined Heating and Power
COP	Coefficient of Performance
DEM	Demand
EPEX	European Power Exchange
FZJ	Forschungszentrum Jülich
GG	Gas Grid
GHG	Greenhouse Gas
GWI	Global Warming Impact
HP	Heat Pump
HPC	High-Performance Computing
HT-ATES	High-temperature ATES
LT-ATES	Low-temperature ATES

MILP	Mixed-Integer Linear Programming
MIQCP	Mixed-Integer Quadratically Constrained Programming
OPEX	Operational Expenditures
PG	Power Grid
PV	Photovoltaic
SOC	State of Charge
TAC	Total Annualized Costs
WH	Waste Heat Source

Greek Symbols

Δ	Difference [-]
η	Efficiency [-]
γ	Maintenance coefficient [-]
λ	Part load [-]
τ	Time constant [s]

Latin Symbols

b	Build/operational decision [-]
C	Specific cost [€/MW]
c_p	Specific heat capacity [kJ/kgK]
E	Capacity [MWh]
g	Gravity factor [m/s^2]
h	Aquifer depth [m]
I	Solar irradiance [kW/m^2]
i	Interest rate [-]
j, k	Counting variables
$\dot{m}$	Mass flow rate [kg/s]
$\mathcal{N}$	Set of additional components [-]
n	Time horizon [-]
P	Electric power [MW]
$\dot{Q}$	Thermal power [MW]
$\mathcal{T}$	Set of all considered time points [-]
T	Temperature [K]
$\mathcal{U}$	Set of existing components [-]
w	Weighting factor [-]

Subscripts and Superscripts

C	Cold
ch	Charge
cond	Condenser
dis	Discharge
el	Electrical
evap	Evaporator
H	Hot
in	Input
max	Maximal
min	Minimal
nom	Nominal
op	Operation
out	Output
pl	Part-load

Appendix A. Maintenance Costs

Table A1. Maintenance costs for the existing components

Component	**Reference costs [k€]**	**Maintenance coefficient γ**
AC	1030	0.01
B	450	0.015
CC	0	0
CHP	1684.2	0.1
PV	1150	0.01

Appendix B. Input Data

Table B1. Cluster centers of the dataset with peak values

Heating [MW]	Cooling [MW]	Power [MW]	Solar [kW/m²]	Flow T [K]	Return T [K]	Ambient T [K]	Gas price [€/MWh]	Electricity price [€/MWh]	Month	dt
36.619	6.961	21.543	0.893	391.55	328.65	265.18	49.46	2325.83	0	0.0
21.839	3.645	11.780	0.0361	385.62	336.06	272.25	31.48	91.06	1	386.0
13.430	4.047	11.953	0.0452	372.64	334.89	281.89	29.20	60.95	1	358.0
11.019	3.866	11.671	0.0633	369.68	336.05	283.40	26.33	57.41	2	470.0
15.783	3.811	11.800	0.0343	377.92	336.19	278.03	25.41	69.50	2	226.0
13.165	3.953	11.475	0.0443	373.47	336.16	280.74	26.63	67.12	3	435.0
8.375	4.335	12.330	0.2124	365.67	337.25	285.84	26.74	61.31	3	309.0
6.240	4.917	13.101	0.2050	363.54	338.72	289.46	27.64	45.44	4	326.0
12.386	4.170	11.948	0.1151	373.41	336.79	280.81	30.07	76.36	4	394.0
4.522	5.435	11.813	0.4344	363.58	336.86	292.90	30.94	29.65	5	269.0
7.096	4.703	11.491	0.0707	365.70	336.02	286.99	31.86	88.48	5	475.0
6.947	4.104	9.771	0.1034	366.53	335.61	286.49	34.53	82.30	6	324.0
4.129	5.303	10.715	0.3431	363.96	337.09	293.24	34.28	88.77	6	396.0
5.037	5.048	10.905	0.0609	364.15	336.66	290.04	32.19	86.56	7	442.0
3.637	6.262	11.148	0.4703	363.73	336.97	296.78	32.10	40.10	7	302.0
3.551	6.578	11.833	0.4497	364.47	337.12	297.74	37.63	46.28	8	309.0
4.552	5.881	11.478	0.0400	364.54	336.82	291.48	37.42	106.17	8	435.0
9.355	4.438	11.418	0.0450	370.58	335.86	283.17	36.55	74.22	9	156.0
5.101	5.674	11.221	0.1791	364.87	337.35	291.39	36.20	79.44	9	564.0
7.243	4.834	11.303	0.1089	364.55	338.89	287.69	40.79	84.14	10	502.0
11.119	4.268	11.263	0.0205	370.97	337.31	282.28	40.26	90.18	10	242.0
11.973	3.889	11.675	0.0454	372.24	336.90	281.77	43.85	113.70	11	563.0
18.127	3.744	11.738	0.0291	382.43	337.56	275.71	47.61	114.64	11	157.0
18.243	3.787	11.442	0.0216	382.46	337.35	275.91	46.38	135.54	12	405.0
13.962	3.978	11.511	0.0265	374.40	336.74	281.13	44.94	75.79	12	339.0

Appendix C. Numerical Results

Table C1. Detailed values of Pareto front for Ref.

	Annual output [GWh]						
Solution	**CHP**	**B**	**CC**	**AC**	**PV**	**GWI [kt$_{CO_2}$/a]**	**TAC [Mio.€/a]**
1	128.0	26.84	31.85	8.84	1.88	36.72	24.78
2	147.3	18.12	32.03	8.66	1.88	38.92	24.06
3	164.6	11.14	31.52	9.17	1.88	41.12	23.70
4	174.3	11.14	28.23	12.46	1.88	43.32	23.48
5	183.9	11.14	24.95	15.74	1.88	45.52	23.35
6	193.6	11.14	21.65	19.04	1.88	47.72	23.26

Table C2. Detailed values of Pareto front for CS_I

	Annual output [GWh]									
Solution	**CHP**	**B**	**CC**	**AC**	**PV**	**HP$_{WH}$**	**HP$^{ch}_{ATES}$**	**HP$^{dis}_{ATES}$**	**GWI [kt$_{CO_2}$/a]**	**TAC [Mio.€/a]**
1	124.4	1.24	31.26	9.43	1.88	21.2	6.13	6.71	29.47	25.05
2	140.4	1.30	31.26	9.43	1.88	20.81	/	/	33.14	24.12
3	156.4	1.39	27.52	13.17	1.88	18.51	/	/	36.80	23.75
4	172.5	1.39	25.94	14.75	1.88	13.51	/	/	40.47	23.47
5	183.7	5.89	25.82	14.87	1.88	4.28	/	/	44.13	23.30
6	199.5	6.14	21.02	19.67	1.88	3.38	/	/	47.80	23.16

Table C3. Design values for CS_I.

	Design value [MW]					
Solution	**ATES**	**HP$_{ATES}$**	**HP$_{WH}$**	**E$_{ATES}$ [MWh]**	**T$_{H,charge}$ [°C]**	**T$_{H,discharge}$ [°C]**
1	4.01	5.23	5.7	5134	80	65
2	/	/	5.7	/	/	/
3	/	/	5.48	/	/	/
4	/	/	5.48	/	/	/
5	/	/	1.47	/	/	/
6	/	/	1.23	/	/	/

Table C4. Detailed values of Pareto front for CS_{II}.

	Annual output [GWh]							
Solution	**B**	**CC**	**PV**	**HP$_{WH}$**	**HP$^{ch}_{ATES}$**	**HP$^{dis}_{ATES}$**	**GWI [kt$_{CO_2}$/a]**	**TAC [Mio.€/a]**
1	12.65	40.69	1.88	44.59	23.92	27.22	3.18	26.28
2	16.38	40.69	1.88	46.69	18.51	21.39	4.12	25.94
3	20.11	40.69	1.88	46.68	15.45	17.67	5.05	25.89
4	23.82	40.69	1.88	47.14	11.81	13.48	5.99	25.83
5	27.56	40.69	1.88	47.06	8.55	9.83	6.92	25.78
6	31.29	40.69	1.88	46.91	5.40	6.26	7.86	25.75

Table C5. Design values for CS_{II}.

	Design value [MW]					
Solution	**ATES**	**HP$_{ATES}$**	**HP$_{WH}$**	**E$_{ATES}$ [MWh]**	**T$_{H,charge}$ [°C]**	**T$_{H,discharge}$ [°C]**
1	8.08	10.74	6.10	16 990	75	60
2	5.24	6.55	5.84	11 122	80	65
3	4.30	5.33	5.80	9491	80	65
4	3.11	3.81	5.93	6721	80	65
5	2.22	2.70	5.82	4789	80	65
6	1.28	1.56	5.82	2844	80	65

Table C6. Detailed values of Pareto front for S_I

Annual output [GWh]										
Solution	**CHP**	**B**	**CC**	**AC**	**PV**	**HP_{WH}**	**HP^{ch}_{ATES}**	**HP^{dis}_{ATES}**	**GWI [kt_{CO_2}/a]**	**TAC [Mio.€/a]**
1	124.4	1.24	31.26	9.43	1.88	19.31	8.21	8.60	29.47	25.04
2	140.4	1.30	31.26	9.43	1.88	20.81	/	/	33.14	24.12
3	156.4	1.39	27.52	13.17	1.88	18.51	/	/	36.80	23.75
4	172.5	1.39	25.94	14.75	1.88	13.51	/	/	40.47	23.47
5	183.7	5.89	25.82	14.87	1.88	4.28	/	/	44.13	23.30
6	199.5	6.14	21.02	19.67	1.88	3.38	/	/	47.80	23.16

Table C7. Design values for S_I.

Design value [MW]						
Solution	**ATES**	**HP_{ATES}**	**HP_{WH}**	**E_{ATES} [MWh]**	**$T_{H,charge}$ [°C]**	**$T_{H,discharge}$ [°C]**
1	4.09	5.23	5.7	6825	80	70
2	/	/	5.7	/	/	/
3	/	/	5.48	/	/	/
4	/	/	5.48	/	/	/
5	/	/	1.47	/	/	/
6	/	/	1.23	/	/	/

Table C8. Detailed values of Pareto front for S_{II}

Annual output [GWh]										
Solution	**CHP**	**B**	**CC**	**AC**	**PV**	**HP_{WH}**	**HP^{ch}_{ATES}**	**HP^{dis}_{ATES}**	**GWI [kt_{CO_2}/a]**	**TAC [Mio.€/a]**
1	124.4	1.24	31.26	9.43	1.88	21.2	6.13	6.71	29.47	29.46
2	133.5	1.24	31.61	9.08	1.88	21.7	1.55	1.73	31.54	28.96
3	142.5	1.30	30.02	10.67	1.88	21.55	/	/	33.61	28.75
4	151.6	1.30	28.98	11.71	1.88	18.83	/	/	35.68	28.65
5	160.7	1.30	27.87	12.82	1.88	16.24	/	/	37.75	28.59
6	169.7	1.39	26.69	14.00	1.88	13.72	/	/	39.82	28.55

Table C9. Design values for S_{II}.

Design value [MW]						
Solution	**ATES**	**HP_{ATES}**	**HP_{WH}**	**E_{ATES} [MWh]**	**$T_{H,charge}$ [°C]**	**$T_{H,discharge}$ [°C]**
1	4.01	5.23	5.7	5134	80	65
2	0.83	1.08	5.7	1069	80	65
3	/	/	5.7	/	/	/
4	/	/	5.7	/	/	/
5	/	/	5.7	/	/	/
6	/	/	5.48	/	/	/

References

1. European Commission. European Climate Law. https://climate.ec.europa.eu/eu-action/european-climate-law_en (accessed on 16.10.2025).
2. International Energy Agency (IEA). Energy and AI: World energy special outlook report. Technical report, IEA, 2025. https://iea.blob.core.windows.net/assets/ed0483fd-aab4-4cf9-b25a-5aa362b56a2f/EnergyandAI.pdf (accessed on 15.10.2025).
3. Yuan, X.; Liang, Y.; Hu, X.; Xu, Y.; Chen, Y.; Kosonen, R. Waste heat recoveries in data centers: A review. *Renewable and Sustainable Energy Reviews* **2023**, *188*, 113777. https://doi.org/https://doi.org/10.1016/j.rser.2023.113777.
4. Stock, J.; Arjuna, F.; Xhonneux, A.; Müller, D. Modelling of waste heat integration into an existing district heating network operating at different supply temperatures. *Smart Energy* **2023**, *10*, 100104. https://doi.org/10.1016/j.segy.2023.100104.
5. Herrmann, M.; Fleuchaus, P.; Godschalk, B.; Verbiest, M.; Niemi Sørensen, S.; Blum, P. Capital costs of aquifer thermal energy storage (ATES): a review. *Renewable and Sustainable Energy Reviews* **2026**, *226*, 116202. https://doi.org/10.1016/j.rser.2025.116202.
6. Stemmle, R.; Blum, P.; Schüppler, S.; Fleuchaus, P.; Limoges, M.; Bayer, P.; Menberg, K. Environmental impacts of aquifer thermal energy storage (ATES). *Renewable and Sustainable Energy Reviews* **2021**, *151*, 111560. https://doi.org/https://doi.org/10.1016/j.rser.2021.111560.
7. Fleuchaus, P.; Schüppler, S.; Stemmle, R.; Menberg, K.; Blum, P. Aquiferspeicher in Deutschland. *Grundwasser* **2021**, *26*, 123–134. https://doi.org/10.1007/s00767-021-00478-y.

8. Jackson, M.D.; Regnier, G.; Staffell, I. Aquifer Thermal Energy Storage for low carbon heating and cooling in the United Kingdom: Current status and future prospects. *Applied Energy* **2024**, *376*, 124096. https://doi.org/https://doi.org/10.1016/j.apenergy.2024.124096.
9. International Energy Agency (IEA). Energy storage: Country Report Netherlands. Technical report, IEA, 2021. https://iea-es.org/wp-content/uploads/public/Netherlands_Country_Report_2021.pdf (accessed on 16.10.2025.
10. Stemmle, R.; Arab, A.; Bauer, S.; Beyer, C.; Blöcher, G.; Bossennec, C.; Dörnbrack, M.; Hahn, F.; Jaeger, P.; Kranz, S.; et al. Current research on aquifer thermal energy storage (ATES) in Germany. *Grundwasser* **2025**. https://doi.org/10.1007/s00767-025-00590-3.
11. Regnier, G.; Salinas, P.; Jacquemyn, C.; Jackson, M.D. Numerical simulation of aquifer thermal energy storage using surface-based geologic modelling and dynamic mesh optimisation. *Hydrogeology Journal* **2022**, *30*, 1179–1198. https://doi.org/10.1007/s10040-022-02481-w.
12. Daniilidis, A.; Mindel, J.; Filho, F.d.O.; Guglielmetti, L. Techno-economic assessment and operational CO2 emissions of High-Temperature Aquifer Thermal Energy Storage (HT-ATES) using demand-driven and subsurface-constrained dimensioning. *Energy* **2022**, *null*, null. https://doi.org/10.1016/j.energy.2022.123682.
13. Schüppler, S.; Fleuchaus, P.; Blum, P. Techno-economic and environmental analysis of an Aquifer Thermal Energy Storage (ATES) in Germany. *Geothermal Energy* **2019**, *7*, 11. https://doi.org/10.1186/s40517-019-0127-6.
14. Todorov, O.; Alanne, K.; Virtanen, M.; Kosonen, R. Aquifer Thermal Energy Storage (ATES) for District Heating and Cooling: A Novel Modeling Approach Applied in a Case Study of a Finnish Urban District. *Energies* **2020**, *13*, 2478. https://doi.org/10.3390/en13102478.
15. Todorov, O.; Alanne, K.; Virtanen, M.; Kosonen, R. A method and analysis of aquifer thermal energy storage (ATES) system for district heating and cooling: A case study in Finland. *Sustainable Cities and Society* **2020**, *53*, 101977. https://doi.org/10.1016/j.scs.2019.101977.
16. Perera, A.; Soga, K.; Xu, Y.; Nico, P.S.; Hong, T. Enhancing flexibility for climate change using seasonal energy storage (aquifer thermal energy storage) in distributed energy systems. *Applied Energy* **2023**, *340*, 120957. https://doi.org/10.1016/j.apenergy.2023.120957.
17. Verheyen, J.; Thommessen, C.; Roes, J.; Hoster, H. Effects on the Unit Commitment of a District Heating System Due to Seasonal Aquifer Thermal Energy Storage and Solar Thermal Integration. *Energies* **2025**, *18*, 645. https://doi.org/10.3390/en18030645.
18. Dvorak, V.; Zavrel, V.; Torrens Galdiz, J.I.; Hensen, J.L.M. Simulation-based assessment of data center waste heat utilization using aquifer thermal energy storage of a university campus. *Building Simulation* **2020**, *13*, 823–836. https://doi.org/10.1007/s12273-020-0629-y.
19. Leindals, L.; Grønning, P.; Dominković, D.F.; Junker, R.G. Context-aware reinforcement learning for cooling operation of data centers with an Aquifer Thermal Energy Storage. *Energy and AI* **2024**, *17*, 100395. https://doi.org/10.1016/j.egyai.2024.100395.
20. Remmelts, J.; Tensen, S.; Ferreira, C.I. Seasonal thermal energy storage for large scale district heating **2020**.
21. Langiu, M.; Shu, D.Y.; Baader, F.J.; Hering, D.; Bau, U.; Xhonneux, A.; Müller, D.; Bardow, A.; Mitsos, A.; Dahmen, M. COMANDO: A Next-Generation Open-Source Framework for Energy Systems Optimization. *Computers & Chemical Engineering* **2021**, *152*, 107366. https://doi.org/10.1016/j.compchemeng.2021.107366.
22. Sass, S.; Faulwasser, T.; Hollermann, D.E.; Kappatou, C.D.; Sauer, D.; Schütz, T.; Shu, D.Y.; Bardow, A.; Gröll, L.; Hagenmeyer, V.; et al. Model compendium, data, and optimization benchmarks for sector-coupled energy systems. *Computers & Chemical Engineering* **2020**, *135*, 106760. https://doi.org/10.1016/j.compchemeng.2020.106760.
23. Stock, J.; Berrenberg, M.; Xhonneux, A.; Müller, D. Design and Operational Optimisation of a Combined Cooling, Heating and Power Plant to Enable Waste Heat Integration into an Existing District Heating Network. In Proceedings of the 36th International Conference on Efficiency, Cost, Optimization, Simulation and Environmental Impact of Energy Systems (ECOS 2023), Las Palmas De Gran Canaria, Spain, 2023; pp. 1252–1263. https://doi.org/10.52202/069564-0114.
24. Augenstein, E.; Herbergs, S.; Kuperjans, I.; Lucas, K. SIMULATION OF INDUSTRIAL ENERGY SUPPLY SYSTEMS WITH INTEGRATED COST OPTIMIZATION.
25. Fetting, C. The European green deal. *ESDN report, December* **2020**, *2*, 53. https://www.esdn.eu/fileadmin/ESDN_Reports/ESDN_Report_2_2020.pdf (accessed on 28.10.2025).
26. Bundesamt für Wirtschaft und Ausfuhrkontrolle: Informationsblatt CO2-Faktoren. *Bundesförderung für Energie-und Ressourceneffizienz in der Wirtschaft-Zuschuss* **2024**. https://www.bafa.de/SharedDocs/Downloads/DE/Energie/eew_infoblatt_co2_faktoren_2024.pdf?__blob=publicationFile&v=4 (accessed on 28.10.2025).
27. Hering, D.; Cansev, M.E.; Tamassia, E.; Xhonneux, A.; Müller, D. Temperature control of a low-temperature district heating network with Model Predictive Control and Mixed-Integer Quadratically Constrained Programming. *Energy* **2021**, *224*, 120140. https://doi.org/10.1016/j.energy.2021.120140.
28. REINHOLDT, L.; KRISTOFERSSON, J.; ZÜHLSDORF, B.; Et Al.. Heat pump COP, part 1: generalized method for screening of system integration potentials., 2018. https://doi.org/10.18462/IIR.GL.2018.1380.

29. Pieper, H.; Ommen, T.; Buhler, F.; Paaske, B.L.; Elmegaard, B.; Markussen, W.B. Allocation of investment costs for large-scale heat pumps supplying district heating. *Energy Procedia* **2018**, *147*, 358–367. https://doi.org/10.1016/j.egypro.2018.07.104.
30. Ahrendts, F.; Drechsler, B.; Hendricks, J.; Küpper, J.; Lang, S.; Peil, T.; Scholz, D.; Timofeeva, E.; Utri, M.; Weidinger, L.; et al. Roll-out von Großwärmepumpen in Deutschland, 2023. https://doi.org/10.24406/PUBLICA-1440.
31. Leppänen, T.; Romka, R.; Tervonen, P. Utilization of Data Center Waste Heat in Northern Ostrobothnia. *Tehnički glasnik* **2020**, *14*, 312–317. https://doi.org/10.31803/tg-20200706172649.
32. Bundesministerium der Finanzen. Personalkosten, Sachkosten und Kalkulationszinssätze in der Bundesverwaltung für Wirtschaftlichkeitsuntersuchungen und Kostenberechnungen **2024**. https://www.bundesfinanzministerium.de/Content/DE/Standardartikel/Themen/Oeffentliche_Finanzen/Bundeshaushalt/personalkosten-sachkosten-2024-anl.pdf?__blob=publicationFile&v=6 (accessed on 22.10.2025).
33. Zhou, D.; Li, K.; Gao, H.; Tatomir, A.; Sauter, M.; Ganzer, L. Techno-economic assessment of high-temperature aquifer thermal energy storage system, insights from a study case in Burgwedel, Germany. *Applied Energy* **2024**, *null*, null. https://doi.org/10.1016/j.apenergy.2024.123783.
34. Hering, D.; Faller, M.R.; Xhonneux, A.; Müller, D. Operational optimization of a 4th generation district heating network with mixed integer quadratically constrained programming. *Energy* **2022**, *250*, 123766. https://doi.org/10.1016/j.energy.2022.123766.
35. Hering, D.; Xhonneux, A.; Müller, D. Design optimization of a heating network with multiple heat pumps using mixed integer quadratically constrained programming. *Energy* **2021**, *226*, 120384. https://doi.org/10.1016/j.energy.2021.120384.
36. Gao, L.; Zhao, J.; An, Q.; Wang, J.; Liu, X. A review on system performance studies of aquifer thermal energy storage. *Energy Procedia* **2017**, *142*, 3537–3545. https://doi.org/10.1016/j.egypro.2017.12.242.